



ARTICLE

Chronic α 1-Na/K-ATPase inhibition reverses the elongation of the axon initial segment of the hippocampal CA1 pyramidal neurons in Angelman syndrome model mice

Prudhvi Raj Rayi¹, Alexei Y. Bagrov² and Hanoch Kaphzan¹

Angelman syndrome (AS) is a neurodevelopmental disorder caused by the loss of function of the maternal *UBE3A* gene. The hippocampus is one of the most prominently affected brain regions in AS model mice, manifesting in severe hippocampal-dependent memory and plasticity deficits. Previous studies in AS mice reported an elongated axon initial segment (AIS) in pyramidal neurons (PNs) of the hippocampal CA1 region. These were the first reports in mammals to show AIS elongation in vivo. Correspondingly, this AIS elongation was linked to enhanced expression of the α 1 subunit of Na^+/K^+ -ATPase (α 1-NaKA). Recently, it was shown that selective pharmacological inhibition of α 1-NaKA by marinobufagenin (MBG) in adult AS mice rescued the hippocampal-dependent deficits via normalizing their compromised activity-dependent calcium (Ca^{2+}) dynamics. In the herein study, we showed that a chronic selective α 1-NaKA inhibition reversed the AIS elongation in hippocampal CA1 PNs of adult AS mice, and differentially altered their excitability and intrinsic properties. Taken together, our study is the first to demonstrate in vivo structural plasticity of the AIS in a mammalian model, and further elaborates on the modulatory effects of elevated α 1-NaKA levels in the hippocampus of AS mice.

Neuropsychopharmacology (2021) 46:654–664; <https://doi.org/10.1038/s41386-020-00907-1>

INTRODUCTION

Angelman syndrome (AS) is a neurodevelopmental disorder, which entails severe motor and cognitive impairments [1–3]. The major genetic cause of AS is the loss of function of the maternal ubiquitin-protein ligase E3A (*UBE3A*) gene located in 15q11.2–13.3 region [4–7]. Within the same region, in close proximity to the *UBE3A* gene locus, is the Prader–Willi syndrome (PWS) critical region, which in contrast to AS results from a deletion on the paternal chromosome [8–10]. AS mouse models with *Ube3a* maternal deficiency (m^-/p^+) have recapitulated many of the cardinal features observed in AS patients [11–15]. Some of the noticeable deficits in AS model mice were reported in the hippocampus, such as impairments in long-term potentiation and hippocampal-dependent memory [11, 12, 16–18].

The axon initial segment (AIS) is an important cellular compartment of the neuron located at the start of the axon, just after the axon hillock region [19], and is responsible for the initiation of action potentials (APs) [20–23]. The AIS exhibits structural and functional plasticity in an activity-dependent manner, which fine-tunes the neuronal output, thereby affecting the network [22, 24–28]. This activity-dependent structural plasticity of the AIS triggers homeostatic responses to adapt to the alterations in neuronal excitability [24, 27]. Structural alterations such as changes in AIS length or location have been reported in many pathological conditions [29–34]. One such condition is AS. Previous studies in the AS mouse model have reported an elongated AIS in pyramidal neurons (PNs) of the CA1 hippocampal region [17, 35]. These

studies were the first to identify AIS elongation in vivo in mammals. Further, this AIS elongation was shown to be a homeostatic response to the early increase in the expression levels of the α 1 subunit of Na^+/K^+ -ATPase (α 1-NaKA), which starts at the age of 2 weeks (P14) [17, 35]. Preventing this early enhancement of α 1-NaKA expression in AS mice, via genetic manipulation, averted the later development of impaired hippocampal synaptic plasticity and memory deficits as well as the AIS elongation at the CA1 PNs [17]. A follow-up study demonstrated that as a result of the enhanced α 1-NaKA expression, the activity-dependent calcium (Ca^{2+}) signaling in CA1 PNs of AS mice were also compromised [18]. Moreover, the same study showed that pharmacological intervention with marinobufagenin (MBG), a selective α 1-NaKA inhibitor [18, 36, 37], rescued the already evolved hippocampal-dependent plasticity and memory deficits in adult AS mice via normalizing the compromised activity-dependent Ca^{2+} signaling [18]. However, it was not shown whether this selective α 1-NaKA inhibition also rescues the elongated AIS phenotype in AS mice hippocampus. In the herein study, we aimed to elucidate the effects of selective α 1-NaKA inhibition on AIS morphology. To this extent, we implanted osmotic minipumps subcutaneously (s.c.) to deliver MBG/vehicle chronically for 28 days. We identified that chronic selective inhibition of α 1-NaKA in AS mice during adulthood induced AIS shortening and normalized the AIS of the CA1 PNs to the WT length. In addition, we found that this inhibition differentially altered the excitability and some of the intrinsic properties of the hippocampal CA1 PNs in AS model mice.

¹Sagol Department of Neurobiology, The Integrated Brain and Behavior Research Center, University of Haifa, Haifa 3498838, Israel and ²Sechenov Institute of Evolutionary Physiology and Biochemistry, 194223 St. Petersburg, Russian Federation
Correspondence: Hanoch Kaphzan (hkaphzan@univ.haifa.ac.il)

Received: 13 July 2020 Revised: 1 October 2020 Accepted: 26 October 2020
Published online: 19 November 2020

MATERIALS AND METHODS

Animals

Adult male and female mice (3–4 m.o.) were used for all the experiments. Mice were sex and age-matched and group-housed on a 12 h light/dark cycle with free access to food and water. AS model mice were generated by crossing female *Ube3a* (m^+/p^-) and male *Ube3a* (m^+/p^+) breeders. The female mouse used as a breeder inherited the deletion from a male parent (m^+/p^-), so its behavior would not be affected [11]. For immunostaining of the AIS in the hippocampal CA1 PNs, we used a total of 15 mice (WT vehicle: $N = 4$; WT MBG: $N = 4$; AS vehicle: $N = 4$; AS MBG: $N = 3$). For immunostaining of the AIS in the layer-5 PNs of the somatosensory cortex (SSCtx), we used a total of 12 mice (WT vehicle: $N = 3$; WT MBG: $N = 3$; AS vehicle: $N = 3$; AS MBG: $N = 3$). For electrophysiology experiments following chronic treatment with MBG/vehicle, we used a total of 21 mice (WT vehicle: $N = 6$; WT MBG: $N = 4$; AS vehicle: $N = 6$; AS MBG: $N = 5$).

Chronic MBG application by osmotic minipumps

MBG, a selective α 1-NaKA inhibitor, was produced in crystalline powder form by Alexei Bagrov and prepared as previously described [38]. Chronic MBG application using osmotic minipumps was carried out as previously reported [18]. Briefly, a 10 mM stock solution was prepared by dissolving MBG in 100% DMSO and stored at -80°C until further use. Fresh dilutions of the required concentration of MBG were prepared in saline to a final concentration containing ~ 2 – 2.5% DMSO, corresponding to the weight of the mouse, and filled into the osmotic minipump. The same saline/DMSO mixture without MBG was used as vehicle. MBG/vehicle was delivered chronically via s.c. route, using Alzet osmotic minipumps (#1004, delivery at $0.11 \mu\text{L/h}$, Alzet, Durect, Cupertino, CA) at a dosage of $10 \mu\text{g/kg/day}$. Mice were anesthetized using isoflurane (2.5% induction, 1.8% maintenance, 0.3 L/min), and a patch of hair was shaved from the upper back and the area of interest was sterilized with 70% ethanol. A mid-scapular incision was made and the osmotic minipump filled with MBG/vehicle was implanted, followed by closure of the incision with sutures (Assut, Switzerland). A thermal pad was placed below the mice to maintain the body temperature throughout the procedure. After surgery, the animals were given an analgesic (dipyrone; 200 mg/kg) and an antibiotic (Baytril; 5 mg/kg , b.i.d.) for 3 consecutive days and left to recover for a week. All of the AIS staining experiments were carried out following 28 days of treatment. The electrophysiological experiments were carried out following 28 days up until 33 days of treatment. The osmotic minipumps used in the herein study held enough material to deliver the drug for up to 42 days.

Slice preparation for whole-cell recordings

Mice with osmotic minipumps were deeply anesthetized with a mixture of ketamine (10% , 200 mg/kg , Vetmarket, Israel) and xylazine (10% , 20 mg/kg , Vetmarket, Israel). We utilized the toe-pinch reflex method to assess the proper depth of anesthesia. Following transcardial perfusion with an aerated ice-cold cutting solution containing (in mM): 110 sucrose, 60 NaCl, 3 KCl, 1.25 NaH_2PO_4 , 28 NaHCO_3 , 0.5 CaCl_2 , 7 MgCl_2 , and 5 D-glucose , we rapidly removed the brain. Hippocampal coronal sections of $300 \mu\text{m}$ thickness were prepared with an SMZ7000 vibratome (Campden Instruments, UK) in ice-cold cutting solution and transferred to a holding chamber with warm artificial cerebrospinal fluid (aCSF) containing (in mM): 125 NaCl, 2.5 KCl, 1.25 NaH_2PO_4 , 25 NaHCO_3 , 25 D-glucose , 2 CaCl_2 , and 1 MgCl_2 , maintained at 34°C . After 30 min recovery in warm aCSF, the slices were stored at room temperature (RT, $24 \pm 1^\circ\text{C}$) for a minimum of 1 h for further recovery. The slices were then transferred to the recording chamber for performing whole-cell recordings from hippocampal CA1 PNs. The cutting solution and the aCSF were continuously bubbled with $95\% \text{ O}_2/5\% \text{ CO}_2$ mixture.

Whole-cell electrophysiology

Hippocampal CA1 PNs were illuminated and visualized using infrared differential interference contrast microscopy and identified by their large pyramidal shape and firing pattern. Recordings were carried out at RT. The recording electrodes were pulled from borosilicate glass pipettes (1B150F-4, WPI, Sarasota, FL) with a resistance of 3 – $5 \text{ M}\Omega$ using an electrode puller (P-1000; Sutter Instruments, Navato, CA), and back-filled with K-gluconate-based intracellular solution containing (in mM): 120 K-gluconate, 10 HEPES, 1 MgCl_2 , 0.2 EGTA, 2 Mg-ATP , 0.2 $\text{Na}_3\text{-GTP}$, osmolarity 290 mOsm and pH 7.3 . The seal was ruptured after the cells reached a resistance of $>2 \text{ G}\Omega$. After entering the whole-cell mode, we waited for at least 5 min for the diffusion of the internal solution before making any recordings. The acquisition of all intrinsic properties was carried out in current-clamp mode. Pipette capacitance was $\sim 99\%$ compensated. Series resistance was monitored throughout each experiment, and neurons with series resistance $>25 \text{ M}\Omega$ and/or resting membrane potential (RMP) $> -55 \text{ mV}$ were excluded from the analysis. Junction potential was corrected offline. Recordings were sampled at 50 kHz , digitized by a Digidata 1440 apparatus (Molecular Devices, San Jose, CA), filtered at 10 kHz , and amplified using a Multiclamp 700B amplifier. The data were analyzed offline by Clampfit 10 (Molecular Devices, San Jose, CA). To study membrane excitability, we injected a series of square current pulses ranging from hyperpolarizing current step of -150 pA to a maximum depolarizing current step of 300 pA in increments of 50 pA . We used these traces to generate firing rate curves by determining the AP frequency evoked at each level of the depolarizing steps ranging from 50 to 300 pA . For measuring input resistance and sag percentage (%sag), we utilized traces elicited by -100 pA hyperpolarizing current injection from the above experiment. Input resistance was calculated by linearly fitting voltage change to the injected current. The %sag was measured as $\frac{V_{\text{peak}} - V_{\text{steady state}}}{V_{\text{peak}}} \cdot 100$ (Supplementary Fig. 2D), as previously reported [39]. For studying the intrinsic membrane properties of the neurons, single APs were triggered by injecting square current pulses for 10 ms in 10 pA steps. The single AP with its peak closest to the 5 ms time point from the start of current injection was used to analyze the various AP parameters such as AP threshold, fast afterhyperpolarizing potential (fAHP), AP half-width, maximum rate of rise, and AP amplitude. For defining the AP threshold potential, we considered the point on the AP trace where its first derivative (dV/dt) reached 30 V/s (Supplementary Fig. 2B). The fAHP was calculated as the voltage difference between the AP threshold and the AHP trough within 5 ms from the end of the current step (Supplementary Fig. 2A). The maximum rate of rise was determined as the maximum dV/dt value on the rising phase of the AP. AP amplitude was measured from the threshold to the peak of the AP (Supplementary Fig. 2A). AP half-width was calculated as the AP duration at the half-maximal amplitude (Supplementary Fig. 2A). Medium afterhyperpolarizing potential (mAHP) and slow afterhyperpolarizing potential (sAHP) were recorded by injecting a current pulse of 3000 pA at 50 Hz for 3 s as was previously described by us and others [36, 40, 41]. mAHP was measured from the average RMP (averaged over 100 ms before the start of the first current step) to the first negative voltage peak after the last spike (Supplementary Fig. 2C). sAHP was measured at 1 s from the end of the pulse (Supplementary Fig. 2C). We used about 4 – 5 slices per mouse to record from the hippocampal CA1 PNs. Analyses were performed by an experimenter blinded to the genotype and treatment.

Immunostaining

Mice with osmotic minipumps were deeply anesthetized using a ketamine/xylazine mixture as abovementioned and were perfused first with ice-cold pre-fixative (12 – 15 mL normal saline), followed by ice-cold fixative (10 – 12 mL 1% PFA and 1% sucrose in 0.1 M PB).

The brains were only lightly fixed to facilitate immunostaining of the AIS [42]. After perfusion, the dissected brains were stored in the same fixative for 2–3 h at 4 °C and then immersed in 30% sucrose in 0.1 M PB until the brains sank to the bottom of the containers. The brains were dissected at –20 °C using a cryostat, and 30 μ m coronal sections of the hippocampus and SSCtx were collected either on to slides or transferred to 0.01 M PBS. For immunostaining, the sections were washed (3 \times 10 min) in 0.01 M PBS and blocked for 2 h at RT with 5% normal goat serum and 0.3% Triton X-100 in 0.01 M PBS (0.3% TPBSgs). The slices were then washed (3 \times 10 min) in 0.01 M PBS and incubated overnight at 4 °C in 1:300 mouse anti-ankyrin-G (ank-G) primary antibody (clone N106/36, NeuroMab, Davis, CA) diluted in 0.1% TPBSgs. The next morning, the slices were further washed (3 \times 10 min) in 0.01 M PBS and incubated for 2 h at RT with 1:1000 goat anti-mouse Alexa Fluor[®] 488 secondary antibody (ab150113, Abcam, Cambridge, UK) diluted in 0.1% TPBSgs. Final wash steps were carried out (3 \times 10 min) in 0.01 M PBS to remove excess secondary antibodies, followed by mounting and air drying before covering with anti-fading agent (Fluoroshield[™] with DAPI, Sigma Aldrich, St. Louis, MO). The slices were then sealed with coverslips for imaging.

Confocal imaging

Imaging was performed with a Nikon Ti Eclipse confocal microscope using a 60 \times (1.40 NA) oil objective at the Center for Microscopy and Imaging at the University of Haifa. On average, ~6 slices per mouse for the hippocampal CA1 region, and ~4 slices per mouse for the SSCtx region were imaged. For each slice, a single region of interest (ROI) within these brain regions was randomly chosen for imaging the PNs and their AIS. Scan of DAPI and Alexa 488 signals were acquired sequentially with laser excitation at 406.8 nm and 492.4 nm, respectively. The image scan size was maintained at 1024 \times 1024 pixels with a pixel dwell time of 6.1 μ s. All the slices were imaged at an optical thickness of 0.05 μ m in the z-axis to obtain z-stacks containing 150–200 images per ROI. The laser intensity settings, pinhole, and exposure time were kept identical throughout for all treated and untreated WT and AS slices to avoid bias during image acquisition. All the z-stacks were saved in the native.nd2 format of the microscope and analyzed in Fiji (ImageJ, NIH).

AIS length quantification

The acquired z-stacks of the ROIs containing axons were opened via Fiji (ImageJ, NIH) and were preprocessed by histogram stretching available in the program's standard settings. The length was measured using the simple neurite tracer plugin available in FIJI. Since the AIS of hippocampal CA1 PNs are close and often overlap, the analysis was performed using the z-stacks (Supplementary Fig. 1B, Supplementary Video 1). Anti-ank-G immunofluorescence was uniformly distributed throughout the AIS, providing a stark contrast in fluorescence intensity at the axon hillock to AIS and AIS to distal axon transitions. Three criteria were applied while analyzing the AIS: (1) only AIS with a clearly visible start and a narrow endpoint were considered for the analysis, (2) only axons that can be traced back to their respective somas were taken into consideration, and (3) only AIS longer than 10 μ m were included. We neither classified the AIS depending on their origin nor considered the AIS emanating from interneurons for analysis. For representative images, the z-stacks from each group were collapsed to form a single maximum intensity projection image. All the analyses were carried out by an experimenter blinded to the genotype and treatment.

Statistics

GraphPad Prism 7th edition software (GraphPad Software, La Jolla, CA) was used to perform statistical analyses. Comparisons of treatment (MBG/vehicle) and genotype were analyzed by two-way analysis of variance (ANOVA) for effects of genotype, treatment, and interaction (genotype \times treatment). We utilized Bonferroni's

correction for *post hoc* multiple comparisons, whenever appropriate. For all tests, $*P < 0.05$ (two-sided) was considered significant. The individual values, each obtained from a single cell, are represented as a scatter dot plot with histograms of mean \pm standard error of the mean. All analyses were performed by an experimenter blinded to the genotype and treatment.

Study approval

All the animal experiments were approved by the University of Haifa Institutional Ethics Committee.

RESULTS

Chronic α 1-NaKA inhibition induces AIS shortening in CA1 PNs of AS model mice

Previous studies showed that the AIS of hippocampal CA1 PNs in AS mice are elongated compared to their WT littermates [17, 35]. This AIS elongation is induced by an increase in the α 1-NaKA levels surfacing at P14, before any of the AIS alterations are observed [35]. Utilizing a genetic manipulation to prevent this α 1-NaKA enhancement averted the development of hippocampal-dependent deficits as well as the AIS elongation seen in hippocampal CA1 PNs of AS mice [17]. A recent study showed that selective pharmacological inhibition of α 1-NaKA during adulthood corrected the hippocampal-dependent deficits via normalizing the compromised activity-dependent Ca^{2+} dynamics in AS mice [18], but the effects on the elongated AIS were not studied. Hence, we investigated whether chronic *in vivo* inhibition of α 1-NaKA pump activity also affects the AIS length in hippocampal CA1 PNs of AS mice (Supplementary Fig. 1A). Using the immunofluorescence signals of ank-G (Supplementary Fig. 1B, Supplementary Video 1), we quantified AIS length in hippocampal CA1 PNs [43]. Consistent with the previous reports [17, 35], AIS in hippocampal CA1 PNs of vehicle-treated AS mice were significantly longer compared to the AIS in WT littermates (Fig. 1A–C). However, chronic *in vivo* inhibition of α 1-NaKA activity by treatment with MBG for 28 days resulted in a significant shortening of the AIS in AS mice, reverting it to a comparable length observed in their WT counterparts (Fig. 1A–C). Further, this chronic treatment showed no effect on the AIS length in WT mice (Fig. 1A–C).

Chronic α 1-NaKA pump inhibition does not affect AIS length in layer-5 SSCtx PNs of AS model mice

As opposed to the AIS elongation in the hippocampal CA1 PNs of AS mice, previous studies showed that AIS length remain unaffected in the SSCtx in these mice. This unaltered AIS length was attributed to the enhanced α 1-NaKA expression levels specifically in the hippocampus but not in the SSCtx [17, 35], although UBE3A was absent in both regions of the AS mouse model [44]. Since the SSCtx of AS mice does not show alterations either in α 1-NaKA expression or in AIS morphology, we chose this brain region as an internal control and examined the effects of chronic α 1-NaKA inhibition on the AIS length of layer-5 PNs in this region (Supplementary Fig. 1C, Supplementary Video 2). Coinciding with the previous studies, the AIS length in layer-5 PNs of the SSCtx was comparable between the AS and WT littermates (Fig. 2A–C). Furthermore, in contrast to the hippocampal CA1 PNs, AIS length in SSCtx layer-5 PNs of the AS mice remained unaltered upon chronic MBG treatment (Fig. 2A–C). Finally, similar to the hippocampal CA1 PNs, this chronic treatment showed no effect on the AIS length of these PNs in the WT mice (Fig. 2A–C).

Chronic α 1-NaKA pump inhibition differentially alters the excitability and intrinsic membrane properties of CA1 PNs in AS model mice

Previous studies have reported that the intrinsic membrane properties of hippocampal CA1 PNs in AS mice are altered

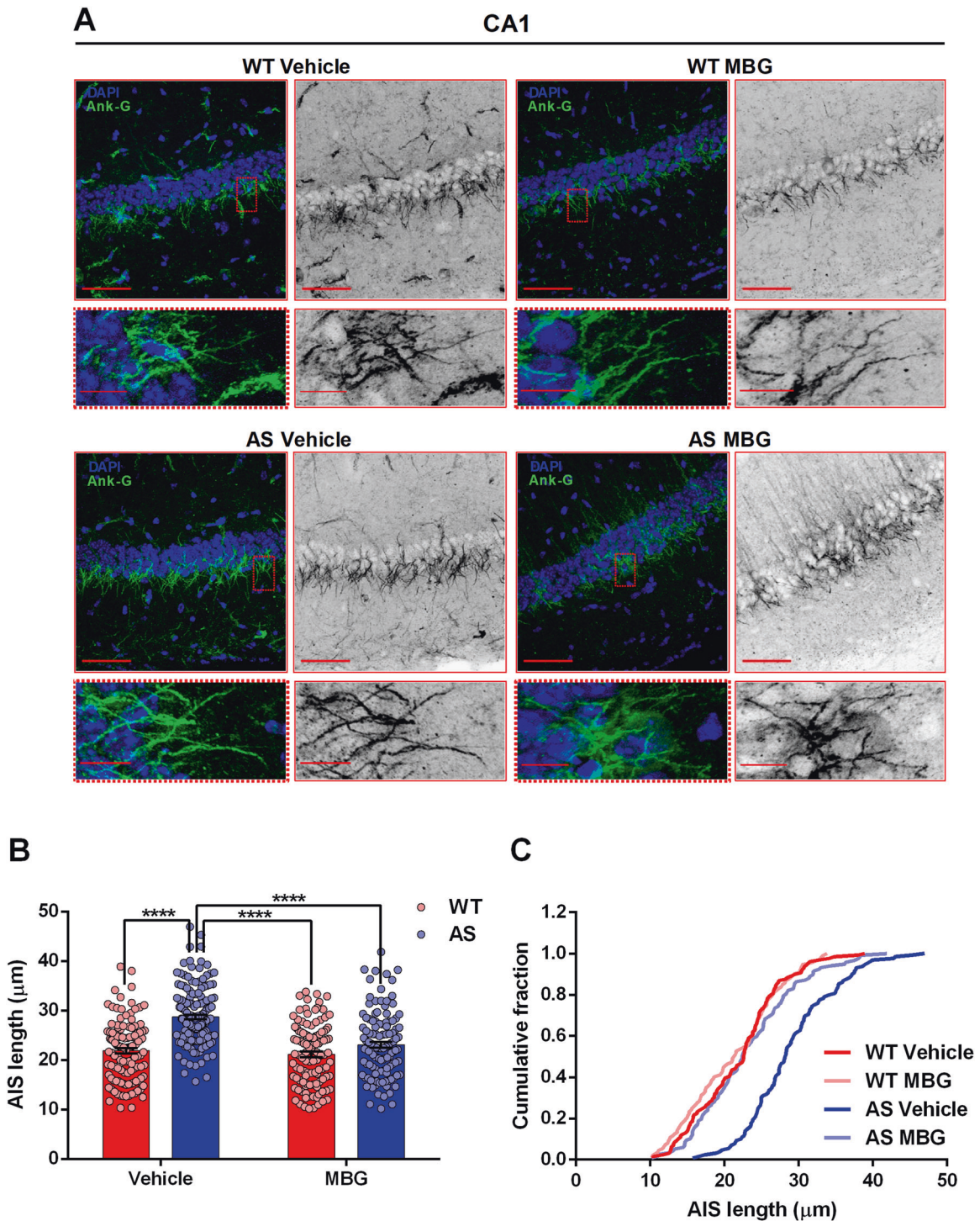


Fig. 1 Chronic selective α 1-NaKA inhibition shortens the elongated AIS of CA1 PNs in AS mice to the WT length. **A** Top: representative collapsed confocal projections of AIS marker ank-G in CA1 PNs in WT and AS mice under different treatment conditions. Scale bar: 50 μ m. Bottom: high resolution magnified scans of the AIS taken from the regions in dotted rectangles (red) in the top panels. Scale bar: 10 μ m. **B** AIS length bar graph with quantified individual CA1 PNs in each of the four conditions. The vehicle-treated AS mice have elongated AIS compared to their WT littermates [$F_{(1, 529)} = 21.43, P < 0.0001$ for interaction of genotype and treatment in two-way ANOVA; *post hoc* Bonferroni corrected comparison of AS vehicle: $t_{(529)} = 9.79, P < 0.0001, t_{(529)} = 10.38, P < 0.0001$ vs. WT vehicle and vs. WT MBG, respectively]. AS mice treated with MBG show a normalized AIS length which is comparable to that of the WT mice [*post hoc* Bonferroni corrected comparison of AS MBG: $t_{(529)} = 7.83, P < 0.0001, t_{(529)} = 1.58, P = 0.70$ vs. AS vehicle and vs. WT vehicle, respectively]. **C** Cumulative frequency distribution (fraction) plot of AIS length in all four conditions. The vehicle-treated AS mice show a right shift toward longer AIS lengths in the distribution curve and MBG-treated AS mice show the entire distribution shifted left toward shorter AIS lengths. For AIS length measurement, WT vehicle: $n = 129$ AIS per region, 4 mice; WT MBG: $n = 112$ AIS per region, 4 mice; AS vehicle: $n = 175$ AIS per region, 4 mice; AS MBG: $n = 117$ AIS per region, 3 mice. Data information: Data are represented as mean \pm SEM and individual data points. **** $P < 0.0001$.

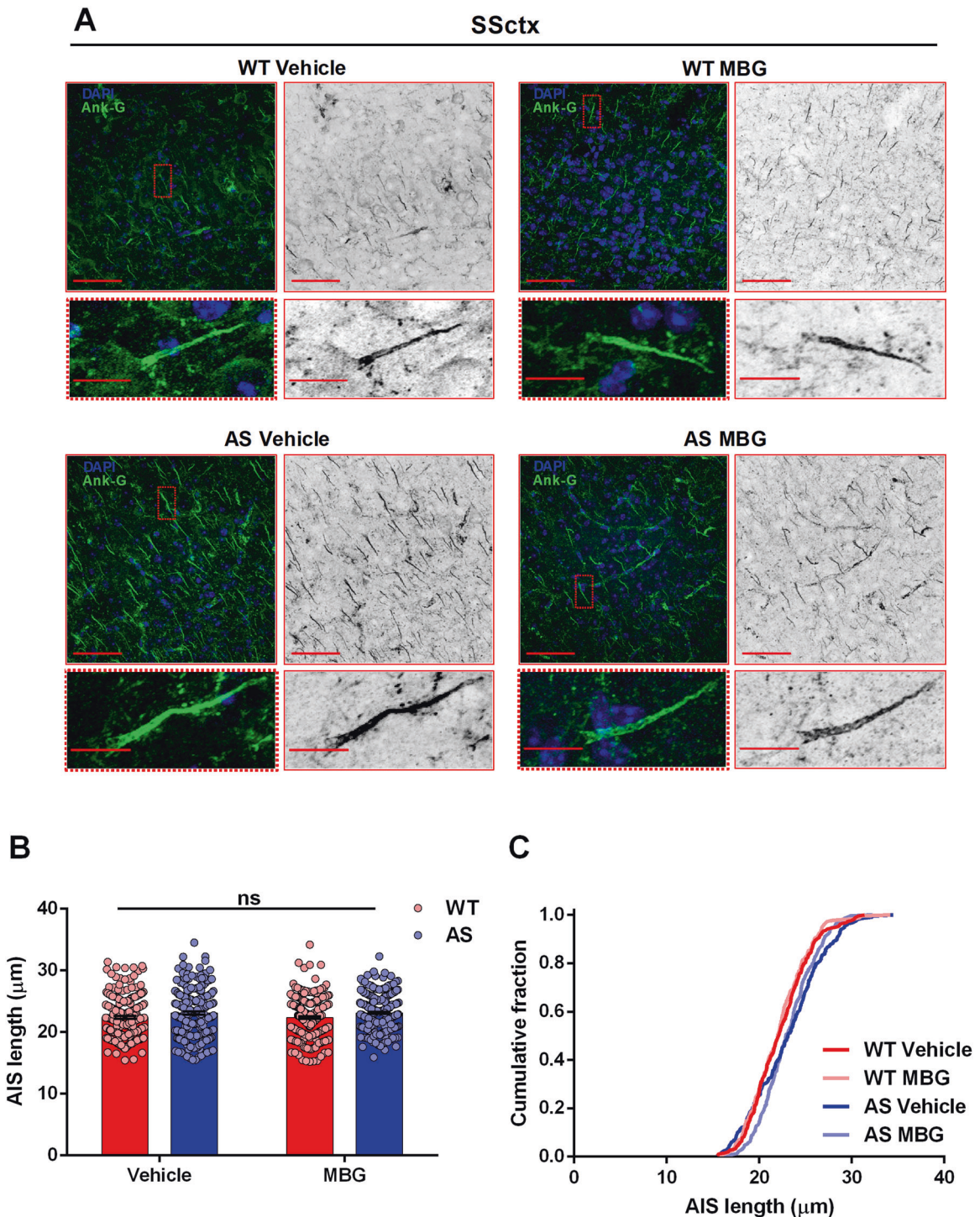


Fig. 2 Chronic selective $\alpha 1$ -NaKA inhibition does not affect AIS length in layer-5 PNs at SSctx of AS mice. **A** Top: representative collapsed confocal projections of AIS marker ank-G in layer-5 PNs of SSctx in WT and AS mice under different treatment conditions. Scale bar: 50 μ m. Bottom: high resolution magnified scans of the AIS taken from the regions in dotted rectangles (red) in the top panels. Scale bar: 10 μ m. **B** AIS length bar graph with quantified individual layer-5 PNs of SSctx in each of the four conditions. AS mice treated with vehicle have similar AIS length compared to their WT littermates [$F_{(1, 930)} = 0.04$, $P = 0.83$ for interaction of genotype and treatment in two-way ANOVA; *post hoc* Bonferroni corrected comparison of AS vehicle: $t_{(930)} = 2.22$, $P = 0.16$, $t_{(930)} = 2.43$, $P = 0.09$ vs. WT vehicle and vs. WT MBG, respectively]. AS and WT mice are not affected by chronic $\alpha 1$ -NaKA inhibition [*post hoc* Bonferroni corrected comparison of AS MBG: $t_{(930)} = 2.57$, $P = 0.06$, $t_{(930)} = 0.14$, $P > 0.9999$ vs. WT MBG and vs. AS vehicle, respectively]. **C** Cumulative frequency distribution (fraction) plot showing no difference in the distribution of AIS length in all four conditions. For AIS length measurement, WT vehicle: $n = 227$ AIS per region, 3 mice; WT MBG: $n = 249$ AIS per region, 3 mice; AS vehicle: $n = 230$ AIS per region, 3 mice; AS MBG: $n = 228$ AIS per region, 3 mice. ns not significant. Data information: Data are represented as mean \pm SEM and individual data points.

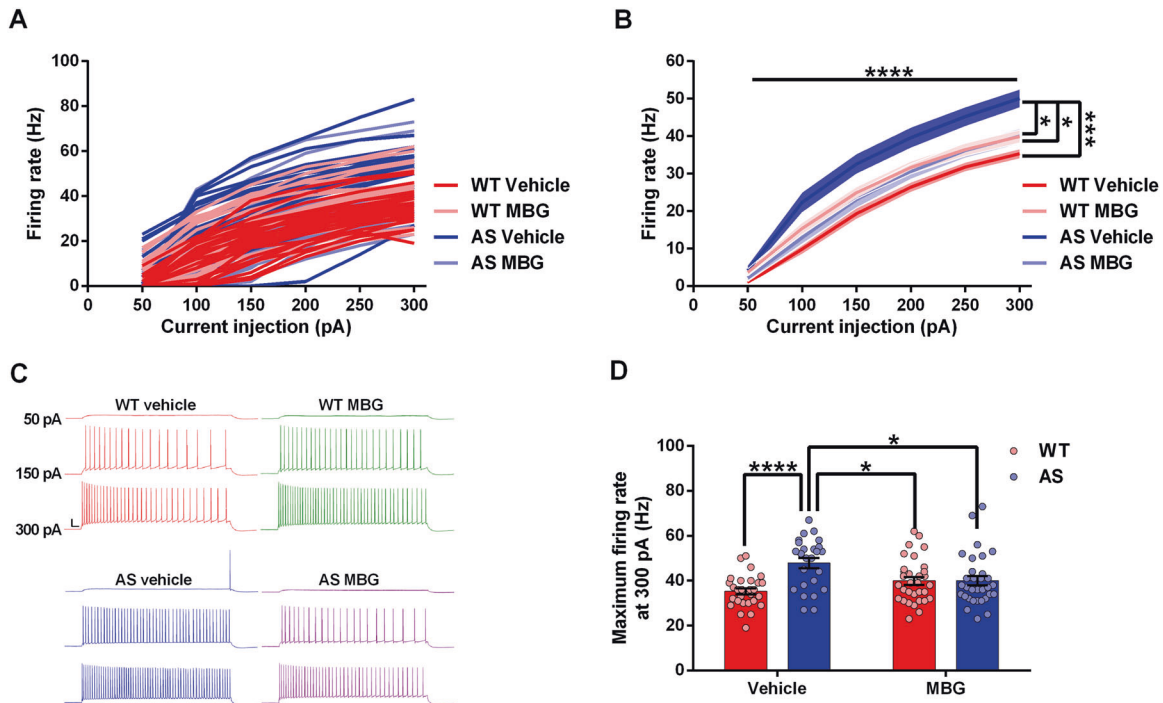
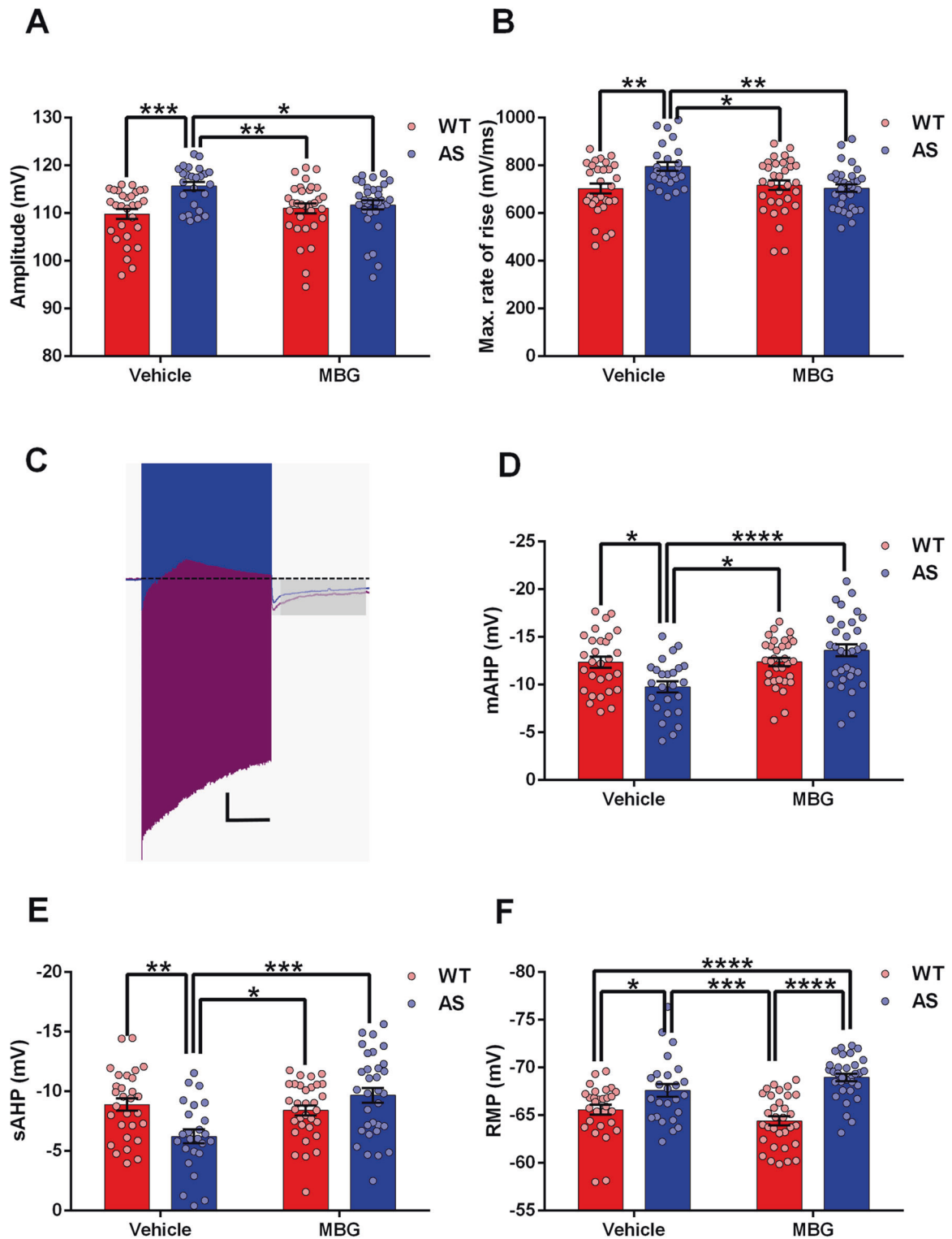


Fig. 3 Chronic selective $\alpha 1$ -NaKA inhibition partially rescues excitability alterations in CA1 PNs of AS model mice. **A** *F-I* curves of individual CA1 PNs from WT and AS mice following chronic MBG/vehicle treatment. **B** Summary of *F-I* curves of all CA1 PNs grouped according to the genotype and treatment. AS vehicle mice exhibit an increase in firing frequency compared to their WT counterparts [$F_{(15,570)} = 4.43$, $P < 0.0001$ for interaction of genotype and current injection in two-way RM ANOVA; *post hoc* Bonferroni corrected comparison of AS vehicle: $t_{(114)} = 4.80$, $P < 0.0001$, $t_{(114)} = 2.93$, $P < 0.05$ vs. WT vehicle and vs. WT MBG, respectively]. MBG treatment significantly lowers the firing rate in AS mice [*post hoc* Bonferroni corrected comparison of AS MBG: $t_{(114)} = 3.42$, $P < 0.01$, $t_{(114)} = 1.55$, $P = 0.75$, vs. AS vehicle and vs. WT vehicle, respectively]. **C** Representative current-clamp recordings of WT and AS mice with MBG/vehicle treatment following injection of 50, 150, and 300 pA current steps. Scale bar: 20 mV, 100 ms. **D** Grouped bar graph showing the maximum firing rate of CA1 PNs at 300 pA current injection in WT and AS mice. AS vehicle mice have significantly higher firing rate than their WT counterparts [$F_{(1, 114)} = 11.30$, $P < 0.01$ for interaction of genotype and treatment in two-way ANOVA; *post hoc* Bonferroni corrected comparison of AS vehicle: $t_{(114)} = 4.58$, $P < 0.0001$, $t_{(114)} = 2.96$, $P < 0.05$ vs. WT vehicle and vs. WT MBG, respectively]. AS MBG mice have a firing rate comparable to that of WT vehicle mice at 300 pA [*post hoc* Bonferroni corrected comparison of AS MBG: $t_{(114)} = 1.83$, $P = 0.42$, $t_{(114)} = 2.93$, $P < 0.05$ vs. WT vehicle and vs. AS vehicle, respectively]. For all parameters, WT vehicle: $n = 29$ cells, 6 mice; WT MBG: $n = 32$ cells, 4 mice; AS vehicle: $n = 25$ cells, 6 mice; AS MBG: $n = 32$ cells, 5 mice. Data information: Data are represented as mean \pm SEM and individual data points. * $P < 0.05$, ** $P < 0.01$, *** $P < 0.001$, **** $P < 0.0001$.

[17, 18, 35]. An early genetic manipulation that prevented the increase in levels of $\alpha 1$ -NaKA averted the development of these aberrant intrinsic properties in adult AS mice [17]. Hence, we aimed to examine whether selective pharmacological inhibition of the $\alpha 1$ -NaKA pump by MBG later in development can reverse these alterations in intrinsic properties after they have fully evolved. To this extent, we measured the electrophysiological properties of hippocampal CA1 PNs *ex vivo* following a chronic *in vivo* treatment with MBG. Firing rate versus current injection (*F-I*) curves of the four conditions showed that AS vehicle mice have increased excitability compared to WT vehicle mice (Fig. 3A–D). Interestingly, chronic MBG treatment showed a partial normalizing effect in AS mice, significantly lowering the firing frequency of hippocampal CA1 PNs closer to the WT mice (Fig. 3B–D). A two-way RM ANOVA of all four groups showed no significant difference between MBG-treated AS mice and vehicle-treated WT mice, as well as between MBG-treated WT mice and the vehicle-treated WT mice (Fig. 3B). This shows that chronic MBG treatment normalized the AP firing rate in AS mice, which was comparable to that of the vehicle-treated WT mice. Nonetheless, an isolated comparison of only AS MBG to WT vehicle group showed a trend for a higher firing rate in the MBG-treated AS mice [$F_{(1,59)} = 2.94$, $P = 0.09$ in two-way RM ANOVA], suggesting that the normalization is not complete. Furthermore, in WT mice, we observed that chronic $\alpha 1$ -NaKA inhibition resulted in an opposite trend toward increasing firing rate. A similar isolated comparison

between WT MBG and WT vehicle showed a significantly higher firing rate for MBG-treated WT mice [$F_{(1, 59)} = 6.42$, $P < 0.05$ in two-way RM ANOVA], which signifies an effect of MBG also on the WT mice (Fig. 3B, D).

In addition to this MBG-induced semi-normalization of the excitability in AS mice, we also observed the effects of chronic MBG treatment on intrinsic membrane properties. Consistent with previous reports, the significantly increased AP amplitude and maximal rate of rise in AS mice [17, 35] were normalized following chronic MBG treatment (Fig. 4A, B). Similarly, we observed that mAHP and sAHP, which were significantly smaller in AS vehicle mice, were normalized entirely to WT levels by chronic MBG treatment (Fig. 4C–E). Coinciding with earlier studies, the RMP was hyperpolarized in AS mice [17, 35]. However, chronic MBG treatment did not affect the RMP in AS and WT littermates (Fig. 4F). We observed an overall treatment effect of MBG on %sag with no significant difference between the groups *post hoc* (Supplementary Fig. 2E). Input resistance was comparable between all the groups irrespective of the treatment (Supplementary Fig. 2F). The AP half-width showed a significant group effect for genotype and treatment with no interaction effect. Further, MBG-treated WT mice showed a significantly lower AP half-width than the AS vehicle mice *post hoc* (Supplementary Fig. 2G). The fAHP was significantly higher only in MBG-treated WT mice but not the vehicle and MBG-treated AS mice (Supplementary Fig. 2H). Consistent with the previous reports [17, 35], we



found a lower threshold potential in the vehicle-treated AS mice, which was not affected by MBG treatment (Supplementary Fig. 2).

DISCUSSION

In this study, we show, for the first time, direct evidence of AIS structural plasticity *in vivo* by selective α 1-NaKA inhibition in AS model mice. Chronic selective pharmacological inhibition of α 1-

NaKA by MBG shortens the elongated AIS in hippocampal CA1 PN of AS mice to the AIS length in WT littermates. Remarkably, this inhibition prompts only a partial rescue of the excitability and intrinsic alterations observed in the hippocampal CA1 PN of AS mice.

Hippocampal phenotypes in AS mice have been extensively studied and replicated [11, 16–18, 45]. One of the most striking alterations observed in these mice is the increase in the AIS length

Fig. 4 Chronic selective $\alpha 1$ -NaKA inhibition differentially rescues the membrane properties of CA1 PNs in AS model mice. **A** Summary bar graph of AP amplitude. AS vehicle mice have a significantly higher AP amplitude when compared to their WT counterparts [$F_{(1, 114)} = 6.70, P < 0.05$ for interaction of genotype and treatment in two-way ANOVA; *post hoc* Bonferroni corrected comparison of AS vehicle: $t_{(114)} = 4.01, P < 0.001, t_{(114)} = 3.28, P < 0.01$ vs. WT vehicle and vs. WT MBG, respectively]. MBG rescues the altered AP amplitude in AS mice, which is comparable to WT mice [*post hoc* Bonferroni corrected comparison of AS MBG: $t_{(114)} = 1.39, P > 0.9999, t_{(114)} = 2.77, P < 0.05$ vs. WT vehicle and vs. AS vehicle, respectively]. **B** Bar graph with scattered data points showing average maximum rate of rise. AS vehicle mice have significantly higher maximum rate of rise compared to their WT counterparts [$F_{(1, 114)} = 7.81, P < 0.01$ for interaction of genotype and treatment in two-way ANOVA; *post hoc* Bonferroni corrected comparison of AS vehicle: $t_{(114)} = 3.32, P < 0.01, t_{(114)} = 2.85, P < 0.05$ vs. WT vehicle and vs. WT MBG, respectively]. AS MBG mice have a normalized maximum rate of rise which is comparable to WT mice [*post hoc* Bonferroni corrected comparison of AS MBG: $t_{(114)} = 0.07, P > 0.9999, t_{(114)} = 3.33, P < 0.01$ vs. WT vehicle and vs. AS vehicle, respectively]. **C** Representative trace showing mAHP (light gray) and sAHP (dark gray) recordings of CA1 PNs following chronic vehicle (blue) and MBG (purple) treatment in AS mice. The APs are truncated for clarity. Scale bar: 10 mV, 1 s. **D** Bar graph with scattered data points showing average mAHP amplitude from all recorded CA1 PNs following a 28-day treatment with MBG/vehicle. AS mice treated with vehicle have significantly smaller mAHP amplitude compared to their WT counterparts [$F_{(1, 114)} = 11.25, P < 0.01$ for interaction of genotype and treatment in two-way ANOVA; *post hoc* Bonferroni corrected comparison of AS vehicle: $t_{(114)} = 3.10, P < 0.05, t_{(114)} = 3.21, P < 0.05$ vs. WT vehicle and vs. WT MBG, respectively]. AS mice treated with MBG have a normalized mAHP amplitude which is comparable to WT mice [*post hoc* Bonferroni corrected comparison of AS MBG: $t_{(114)} = 1.59, P = 0.69, t_{(114)} = 4.69, P < 0.0001$ vs. WT vehicle and vs. AS vehicle, respectively]. **E** Same as **D** but showing average sAHP amplitude. AS vehicle mice have significantly smaller sAHP amplitude when compared to their WT counterparts [$F_{(1, 114)} = 13.04, P < 0.001$ for interaction of genotype and treatment in two-way ANOVA; *post hoc* Bonferroni corrected comparison of AS vehicle: $t_{(114)} = 3.33, P < 0.01, t_{(114)} = 2.78, P < 0.05$ vs. WT vehicle and vs. WT MBG, respectively]. AS mice treated with MBG have a normalized sAHP amplitude which is comparable to WT mice [*post hoc* Bonferroni corrected comparison of AS MBG: $t_{(114)} = 1.02, P > 0.9999, t_{(114)} = 4.38, P < 0.001$ vs. WT vehicle and vs. AS vehicle, respectively]. **F** Summary of RMP of all the CA1 PNs following treatment with MBG/vehicle. AS vehicle mice have a hyperpolarized RMP when compared to the corresponding WT mice [$F_{(1, 114)} = 6.28, P < 0.05$ for interaction of genotype and treatment in two-way ANOVA; *post hoc* Bonferroni corrected comparison of AS vehicle: $t_{(114)} = 2.70, P < 0.05, t_{(114)} = 4.35, P < 0.001$ vs. WT vehicle and vs. WT MBG, respectively]. MBG has no effect on the RMP of AS mice [*post hoc* Bonferroni corrected comparison of AS MBG: $t_{(114)} = 4.82, P < 0.0001, t_{(114)} = 1.88, P = 0.38$ vs. WT vehicle and vs. AS vehicle, respectively]. For all parameters, WT vehicle: $n = 29$ cells, 6 mice; WT MBG: $n = 32$ cells, 4 mice; AS vehicle: $n = 25$ cells, 6 mice; AS MBG: $n = 32$ cells, 5 mice. Data information: Data are represented as mean \pm SEM and individual data points. * $P < 0.05$, ** $P < 0.01$, *** $P < 0.001$, **** $P < 0.0001$.

at the hippocampal CA1 PNs [17, 35]. A similar alteration in the AIS length has been previously reported in principal neurons of the medial nucleus of the trapezoid body of AS mice [46]. However, in the AS mice hippocampus, the observed AIS elongation was attributed to a homeostatic adaptation in response to the increased $\alpha 1$ -NaKA levels [17, 35]. A genetic manipulation that prevented this $\alpha 1$ -NaKA increase averted the AIS elongation and the development of hippocampal-dependent behavioral and synaptic deficits in these mice [17]. Correspondingly, our recent study showed that selective pharmacological inhibition of $\alpha 1$ -NaKA in adulthood also rescued the already evolved hippocampal-dependent synaptic and behavioral phenotypes in AS mice [18]. Given these reports, we hypothesized that chronic pharmacological inhibition of $\alpha 1$ -NaKA beyond the critical period of development might likewise rescue the elongated AIS phenotype of the hippocampal CA1 PNs in AS mice. Using the widely reported AIS marker, ank-G [47, 48], we measured the AIS length following 28 days of treatment with MBG, a selective pharmacological inhibitor of $\alpha 1$ -NaKA [18, 36, 37]. Consistent with previous reports, we found that AS mice have elongated AIS in the CA1 PNs [17, 35] (Fig. 1). As posited, we observed that chronic selective $\alpha 1$ -NaKA inhibition induced a shortening of the AIS in AS mice, leading to their normalization to the length observed in WT littermates (Fig. 1B, C). The exact mechanism by which chronic $\alpha 1$ -NaKA inhibition rescues these AIS alterations is still elusive. However, our previous study showed that the selective inhibition of $\alpha 1$ -NaKA pump resulted in an enhanced RMP depolarization in CA1 PNs of AS model mice compared to their WT counterparts, and rescued the hippocampal-dependent learning and synaptic transmission deficits via normalizing the aberrant activity-dependent Ca^{2+} dynamics [18]. Nonetheless, the *ex vivo* measurements of the RMP in the herein study showed no depolarization (Fig. 4F), probably because MBG was not present during recordings. MBG was not added to the bath during recordings, and the remaining MBG from the *in vivo* treatment was most likely washed out during the different stages of slice production (brain perfusion, slicing in cutting solution, incubation in aCSF in the holding chamber followed by incubation in the recording chamber). Several studies demonstrated that a prolonged

depolarization or modifications in intracellular Ca^{2+} levels could affect AIS plasticity by triggering homeostatic responses such as relocating the AIS or reducing the AIS length within few hours to days [24, 49–51]. Therefore, it is plausible that the *in vivo* chronic selective $\alpha 1$ -NaKA inhibition induces the AIS shortening by either causing a slight but prolonged depolarization, or modifying the intracellular Ca^{2+} concentrations in the CA1 PNs of AS mice [18]. Coinciding with the rescue of the AIS elongation in CA1 PNs of MBG-treated AS mice, we observed a full normalization in some single spike parameters of these neurons. Chronic MBG treatment lowered the AP amplitude and the AP maximal rate of rise in AS mice (Fig. 4A, B), which can be ascribed to the AIS shortening [27, 52, 53] (Fig. 1). We did not investigate if the AIS shortening in AS mice was accompanied by a shift in its location along the axon [24, 50].

In contrast to the hippocampal CA1 PNs, the PNs of SSCTx in AS mice exhibit neither increased levels of $\alpha 1$ -NaKA expression nor elongated AIS [17, 18, 35], despite the loss of UBE3A in both brain regions [44]. Thus, the PNs of SSCTx serve as an excellent internal control for studying the regulatory role of $\alpha 1$ -NaKA in AIS plasticity. As predicted, the AIS in layer-5 PNs of SSCTx showed no alterations in their length irrespective of the genotype and MBG treatment (Fig. 2B, C). These results coincide with our previous studies that showed that the region-specific alterations in activity-dependent Ca^{2+} dynamics and AIS length are dependent on $\alpha 1$ -NaKA expression levels [17, 18, 35].

The reason for the differential $\alpha 1$ -NaKA expression between the hippocampal CA1 and the SSCTx regions, despite the shared absence of UBE3A, is yet unknown. Moreover, the interaction between UBE3A and $\alpha 1$ -NaKA is also obscure, with conflicting evidence of the interaction and substrate specificity of UBE3A. In our hands, we could not co-precipitate $\alpha 1$ -NaKA with UBE3A [35]. However, one study showed a protein–protein interaction between UBE3A and $\alpha 1$ -NaKA [54], and other studies in a *drosophila* model of duplication 15q syndrome (Dup15q) showed α -NaKA to be a direct substrate of Dube3a, a *drosophila* analog of UBE3A [55, 56]. Nevertheless, further studies are required to reveal the mechanisms leading to the region-specific differences in $\alpha 1$ -NaKA levels in AS mice.

Neuronal hyperexcitability has been previously reported in many neuropsychiatric disorders such as autism, Fragile-X syndrome, and Rett syndrome [57–60]. In AS, cellular hyperexcitability has been shown in several distinct brain regions, including the infralimbic cortex, primary visual cortex, and the hippocampal CA1 [18, 61, 62]. This altered cellular excitability may result from various modifications in the AIS [52]. The AIS is considered to be the subcellular region responsible for the initiation of AP [20–22]. Indeed, numerous studies in mice, birds, and dissociated neuronal cultures have reported a direct relationship between AIS plasticity and the neuronal output at both single-cell and network levels [22, 24–28]. Given the findings from these studies, together with our AIS results, we hypothesized that chronic selective α 1-NaKA inhibition would also affect the physiological properties of CA1 PNs in AS mice. CA1 PNs of vehicle-treated AS mice showed increased excitability (Fig. 3B–D), corresponding to the homeostatic elongation of the AIS resulting from the enhanced expression levels of α 1-NaKA [18, 35]. AS mice chronically treated with MBG showed significantly lower firing rates than the vehicle-treated AS mice (Fig. 3B–D). This is congruent with earlier studies, which reported that the AIS elongation leads to a shorter interspike interval, a larger maximal rate of rise (Fig. 4B), and an increase in excitability [27, 29]. Hence, these data suggest that one possible way by which MBG lowers the firing rate in the AS hippocampal CA1 PNs could be by reducing the AIS length (Fig. 1).

Interestingly, the normalization of the elongated AIS was sufficient to significantly lower but not completely normalize the neuronal hyperexcitability of the CA1 PNs in AS mice (Fig. 3B), suggesting that the structural changes in AIS length alone might not account for the enhanced firing rate. We posit that additional factors such as RMP, mAHP, and sAHP, in combination with the AIS shortening might co-regulate the neuronal excitability [18, 22, 35, 49, 63–66]. Indeed, chronic selective α 1-NaKA inhibition with MBG fully normalized the reduced mAHP and sAHP of AS mice (Fig. 4C–E). The mAHP and sAHP are key components of AP firing that determine intrinsic neuronal excitability by mediating spike frequency adaptation in multiple neuronal types [67, 68]. Given that mAHP and sAHP arise from the activity of different channel conductances [40, 63, 69–71], our results suggest that MBG affects these channels as well. A possible additional explanation to the partial normalization of excitability in AS mice is that chronic MBG treatment might have affected α 1-NaKA levels, or the expression of any other excitability-related proteins (channels or pumps). Therefore, the precise mechanism by which chronic α 1-NaKA inhibition differentially regulates excitability is probably heterogeneous and still needs to be determined.

It is noteworthy that the alterations in the intrinsic properties, such as hyperpolarized RMP (Fig. 4F), increased AP amplitude (Fig. 4A), and the higher maximal rate of rise (Fig. 4B) are similar between CA1 PNs and MNTB neurons of the calyx of Held in AS mice [17, 35, 46]. However, it is not known if the principal neurons of MNTB have elevated α 1-NaKA expression levels. The data from our previous study [18] and the herein study suggest that MBG predominantly affects the regions with elevated α 1-NaKA levels. Therefore, if the more hyperpolarized RMP in the principal neurons of MNTB arises from increased expression levels of α 1-NaKA, MBG might also affect the AIS of MNTB neurons similar to that of the CA1 PNs (Fig. 1). However, experimental evidence is still needed.

Given our results, it is reasonable that any intervention that will modulate the AIS morphology will affect the neuronal output and fine-tune the entire network activity. Consequently, the AIS structural plasticity can serve not only as a marker for pathological brain conditions but also as a future therapeutic target. Remarkably, the same MBG application that normalized the elongated AIS phenotype in AS mice (Fig. 1) has previously been

shown to rescue the hippocampal-dependent behavioral deficits of these mice [18].

Overall, our findings reiterate the role of α 1-NaKA overexpression in AS mouse pathophysiology [17, 18, 35] and highlight the possible therapeutic characteristics of selective α 1-NaKA inhibition in rescuing the hippocampal AS phenotypes, extending well beyond the early critical developmental period [18]. The significance of our results may expand beyond AS, notably other neuropsychiatric disorders which entail alterations in NaKA levels, such as autism spectrum disorders and schizophrenia [72–74]. Likewise, our results might also be relevant to chronic brain disorders where AIS abnormalities are implicated, such as schizophrenia [32] or epilepsy [30, 31, 33]. Finally, the herein study provides the first evidence for AIS structural plasticity in vivo in a mammalian model and suggests novel insights into its underlying mechanisms.

FUNDING AND DISCLOSURE

This work was supported by the Israel Science Foundation (grant number 248/20) and by the Angelman syndrome foundation (ASF). The authors declare no competing interests.

DATA AVAILABILITY

All data presented in this study can be obtained from the corresponding author upon request.

AUTHOR CONTRIBUTIONS

PRR performed all the experiments. PRR and HK designed and analyzed the AIS experiments; PRR and HK designed and analyzed the electrophysiology experiments; HK conceptualized all the experiments; AYB extracted the marinobufagenin; PRR and HK wrote the manuscript.

ADDITIONAL INFORMATION

Supplementary Information accompanies this paper at (<https://doi.org/10.1038/s41386-020-00907-1>).

Publisher's note Springer Nature remains neutral with regard to jurisdictional claims in published maps and institutional affiliations.

REFERENCES

1. Clayton-Smith J, Laan L. Angelman syndrome: a review of the clinical and genetic aspects. *J Med Genet.* 2003;40:87–95.
2. Williams CA, Beaudet AL, Clayton-Smith J, Knoll JH, Kyllerman M, Laan LA, et al. Angelman syndrome 2005: updated consensus for diagnostic criteria. *Am J Med Genet A.* 2006;140:413–8.
3. Bindels-de Heus KGCB, Mous SE, ten Hooven-Radstaake M, van Iperen-Kolk BM, Navis C, Rietman AB, et al. An overview of health issues and development in a large clinical cohort of children with Angelman syndrome. *Am J Med Genet Part A.* 2019;182:53–63.
4. Kishino T, Lalonde M, Wagstaff J. UBE3A/E6-AP mutations cause Angelman syndrome. *Nat Genet.* 1997;15:70–3.
5. Matsuura T, Sutcliffe JS, Fang P, Galjaard R-J, Jiang Y, Benton CS, et al. De novo truncating mutations in E6-AP ubiquitin-protein ligase gene (UBE3A) in Angelman syndrome. *Nat Genet.* 1997;15:74–7.
6. Sutcliffe JS, Jiang YH, Galjaard RJ, Matsuura T, Fang P, Kubota T, et al. The E6-AP ubiquitin protein ligase (UBE3A) gene is localized within a narrowed Angelman syndrome critical region. *Genome Res.* 1997;7:368–77.
7. Magenis RE, Brown MG, Lacy DA, Budden S, LaFranchi S. Is Angelman syndrome an alternative result of del(15)(q11q13)? *Am J Med Genet.* 1987;28:829–38.
8. Glenn CC, Driscoll DJ, Yang TP, Nicholls RD. Genomic imprinting: potential function and mechanisms revealed by the Prader-Willi and Angelman syndromes. *Mol Hum Reprod.* 1997;3:321–32.
9. David H, Ledbetter BS, Vincent M, Riccardi MD, Susan D, Airhart BS, et al. Deletions of chromosome 15 as a cause of the Prader-Willi syndrome. *N Engl J Med.* 1991;304:325–9.

10. Knoll JHM, Nicholls RD, Magenis RE, Graham JM, Lalande M, Latt SA, et al. Angelman and Prader-Willi syndromes share a common chromosome 15 deletion but differ in parental origin of the deletion. *Am J Med Genet.* 1989;32:285–90.
11. Jiang YH, Armstrong D, Albrecht U, Atkins CM, Noebels JL, Eichele G, et al. Mutation of the Angelman ubiquitin ligase in mice causes increased cytoplasmic p53 and deficits of contextual learning and long-term potentiation. *Neuron.* 1998;21:799–811.
12. Miura K, Kishino T, Li E, Webber H, Dikkes P, Holmes GL, et al. Neurobehavioral and electroencephalographic abnormalities in Ube3a maternal-deficient mice. *Neurobiol Dis.* 2002;9:149–59.
13. Heck DH, Zhao Y, Roy S, Ledoux MS, Reiter LT. Analysis of cerebellar function in Ube3a-deficient mice reveals novel genotype-specific behaviors. *Hum Mol Genet.* 2008;17:2181–9.
14. Colas D, Wagstaff J, Fort P, Salvat D, Sarda N. Sleep disturbances in Ube3a maternal-deficient mice modeling Angelman syndrome. *Neurobiol Dis.* 2005;20:471–8.
15. Silva-Santos S, van Woerden GM, Bruinsma CF, Mientjes E, Jolfaei MA, Distel B, et al. Ube3a reinstatement identifies distinct developmental windows in a murine Angelman syndrome model. *J Clin Invest.* 2015;125:2069–76.
16. van Woerden GM, Harris KD, Hojjati MR, Gustin RM, Qiu S, de Avila Freire R, et al. Rescue of neurological deficits in a mouse model for Angelman syndrome by reduction of α CaMKII inhibitory phosphorylation. *Nat Neurosci.* 2007;10:280–2.
17. Kaphzan H, Buffington SA, Ramaraj AB, Lingrel JB, Rasband MN, Santini E, et al. Genetic reduction of the $\alpha 1$ subunit of Na/K-ATPase corrects multiple hippocampal phenotypes in Angelman syndrome. *Cell Rep.* 2013;4:405–12.
18. Rayi PR, Koyavski L, Chakraborty D, Bagrov A, Kaphzan H. $\alpha 1$ -Na/K-ATPase inhibition rescues aberrant dendritic calcium dynamics and memory deficits in the hippocampus of an Angelman syndrome mouse model. *Prog Neurobiol.* 2019;182:101676.
19. Palay SL, Sotelo C, Peters A, Orkand PM. The axon hillock and the initial segment. *J Cell Biol.* 1968;38:193–201.
20. Palmer LM, Stuart GJ. Site of action potential initiation in layer 5 pyramidal neurons. *J Neurosci.* 2006;26:1854–63.
21. Kole MHP, Ilshner SU, Kampa BM, Williams SR, Ruben PC, Stuart GJ. Action potential generation requires a high sodium channel density in the axon initial segment. *Nat Neurosci.* 2008;11:178–86.
22. Kuba H, Ishii TM, Ohmori H. Axonal site of spike initiation enhances auditory coincidence detection. *Nature.* 2006;444:1069–72.
23. Araki T, Otani T. Response of single motoneurons to direct stimulation in toad's spinal cord. *J Neurophysiol.* 1955;18:472–85.
24. Grubb MS, Burrone J. Activity-dependent relocation of the axon initial segment fine-tunes neuronal excitability. *Nature.* 2010;465:1070–4.
25. Yue ZW, Wang YL, Xiao B, Feng L. Axon initial segment structural plasticity is involved in seizure susceptibility in a rat model of cortical dysplasia. *Neurochem Res.* 2018;43:878–85.
26. Ding Y, Chen T, Wang Q, Yuan Y, Hua T. Axon initial segment plasticity accompanies enhanced excitation of visual cortical neurons in aged rats. *Neuroreport.* 2018;29:1537–43.
27. Kuba H, Oichi Y, Ohmori H. Presynaptic activity regulates Na⁺ channel distribution at the axon initial segment. *Nature.* 2010;465:1075–8.
28. Hamada MS, Kole MHP. Myelin loss and axonal ion channel adaptations associated with gray matter neuronal hyperexcitability. *J Neurosci.* 2015;35:7272–86.
29. Baalman KL, Cotton RJ, Rasband SN, Rasband MN. Blast wave exposure impairs memory and decreases axon initial segment length. *J Neurotrauma.* 2013;30:741–51.
30. Marco P, Sola RG, Cajal SRY, DeFelipe J. Loss of inhibitory synapses on the soma and axon initial segment of pyramidal cells in human epileptic peritumoural neocortex: Implications for epilepsy. *Brain Res Bull.* 1997;44:47–66.
31. Ribak CE. Axon terminals of GABAergic chandelier cells are lost at epileptic foci. *Brain Res.* 1985;326:251–60.
32. Cruz DA, Weaver CL, Lovallo EM, Melchitzky DS, Lewis DA. Selective alterations in postsynaptic markers of chandelier cell inputs to cortical pyramidal neurons in subjects with schizophrenia. *Neuropsychopharmacology.* 2009;34:2112–24.
33. Harty RC, Kim TH, Thomas EA, Cardamone L, Jones NC, Petrou S, et al. Axon initial segment structural plasticity in animal models of genetic and acquired epilepsy. *Epilepsy Res.* 2013;105:272–9.
34. Yermakov LM, Drouet DE, Griggs RB, Elased KM, Susuki K. Type 2 diabetes leads to axon initial segment shortening in db/db mice. *Front Cell Neurosci.* 2018;12:1–13.
35. Kaphzan H, Buffington SA, Jung JI, Rasband MN, Klann E. Alterations in intrinsic membrane properties and the axon initial segment in a mouse model of Angelman syndrome. *J Neurosci.* 2011;31:17637–48.
36. Chakraborty D, Fedorova OV, Bagrov AY, Kaphzan H. Selective ligands for Na⁺/K⁺-ATPase α isoforms differentially and cooperatively regulate excitability of pyramidal neurons in distinct brain regions. *Neuropharmacology.* 2017;117:338–51.
37. Fedorova OV, Bagrov AY. Inhibition of Na/K ATPase from rat aorta by two Na/K pump inhibitors, ouabain and marinobufagenin: evidence of interaction with different α -subunit isoforms. *Am J Hypertens.* 1997;10:929–35.
38. Bagrov AY, Roukoyatkina NI, Pinaev AG, Dmitrieva RI, Fedorova OV. Effects of two endogenous Na⁺/K⁺-ATPase inhibitors, marinobufagenin and ouabain, on isolated rat aorta. *Eur J Pharmacol.* 1995;274:151–8.
39. Guan D, Armstrong WE, Foehring RC. Electrophysiological properties of genetically identified subtypes of layer 5 neocortical pyramidal neurons: Ca²⁺ dependence and differential modulation by norepinephrine. *J Neurophysiol.* 2015;113:2014–32.
40. Gulledge AT, Dasari S, Onoue K, Stephens EK, Hasse JM, Avesar D. A sodium-pump-mediated afterhyperpolarization in pyramidal neurons. *J Neurosci.* 2013;33:12025–41.
41. Lander SS, Khan U, Lewandowski N, Chakraborty D, Provenzano FA, Mingote S, et al. Glutamate dehydrogenase-deficient mice display schizophrenia-like behavioral abnormalities and CA1-specific hippocampal dysfunction. *Schizophr Bull.* 2019;45:127–37.
42. Tian C, Wang K, Ke W, Guo H, Shu Y. Molecular identity of axonal sodium channels in human cortical pyramidal cells. *Front Cell Neurosci.* 2014;8:1–16.
43. Hu W, Tian C, Li T, Yang M, Hou H, Shu Y. Distinct contributions of Nav1.6 and Nav1.2 in action potential initiation and backpropagation. *Nat Neurosci.* 2009;12:996–1002.
44. Gustin RM, Bichell TJ, Bubser M, Daily J, Filonova I, Mrelashvili D, et al. Tissue-specific variation of Ube3a protein expression in rodents and in a mouse model of Angelman syndrome. *Neurobiol Dis.* 2010;39:283–91.
45. Kaphzan H, Hernandez P, Jung JI, Cowansage KK, Deinhardt K, Chao MV, et al. Reversal of impaired hippocampal long-term potentiation and contextual fear memory deficits in Angelman syndrome model mice by ErbB inhibitors. *BPS.* 2012;72:182–90.
46. Wang T, van Woerden GM, Elgersma Y, Borst JGG. Enhanced transmission at the calyx of Held synapse in a mouse model for Angelman syndrome. *Front Cell Neurosci.* 2018;11:1–19.
47. Boiko T, Vakulenko M, Ewers H, Chan CY, Norden C, Winckler B. Ankyrin-dependent and -independent mechanisms orchestrate axonal compartmentalization of L1 family members neurofascin and L1/neuron-glia cell adhesion molecule. *J Neurosci.* 2007;27:590–603.
48. Jenkins SM, Bennett V. Ankyrin-G coordinates assembly of the spectrin-based membrane skeleton, voltage-gated sodium channels, and L1 CAMs at Purkinje neuron initial segments. *J Cell Biol.* 2001;155:739–45.
49. Evans MD, Dumitrescu AS, Kruijssen DLH, Taylor SE, Grubb MS. Rapid modulation of axon initial segment length influences repetitive spike firing. *Cell Rep.* 2015;13:1233–45.
50. Muir J, Kittler JT. Plasticity of GABAA receptor diffusion dynamics at the axon initial segment. *Front Cell Neurosci.* 2014;8:1–11.
51. Evans MD, Sammons RP, Lebron S, Dumitrescu AS, Watkins TBK, Uebele VN, et al. Calcineurin signaling mediates activity-dependent relocation of the Axon Initial segment. *J Neurosci.* 2013;33:6950–63.
52. Grubb MS, Shu Y, Kuba H, Rasband MN, Wimmer VC, Bender KJ. Short- and long-term plasticity at the axon initial segment. *J Neurosci.* 2011;31:16049–55.
53. Kole MHP, Letzkus JJ, Stuart GJ. Axon initial segment Kv1 channels control axonal action potential waveform and synaptic efficacy. *Neuron.* 2007;55:633–47.
54. Saez I, Koyuncu S, Gutierrez-Garcia R, Dieterich C, Vilchez D. Insights into the ubiquitin-proteasome system of human embryonic stem cells. *Sci Rep.* 2018;8:1–21.
55. Hope KA, LeDoux MS, Reiter LT. Glial overexpression of Dube3a causes seizures and synaptic impairments in Drosophila concomitant with down regulation of the Na⁺/K⁺ pump ATP α . *Neurobiol Dis.* 2017;108:238–48.
56. Jensen L, Farook MF, Reiter LT. Proteomic profiling in drosophila reveals potential Dube3a regulation of the actin cytoskeleton and neuronal homeostasis. *PLoS ONE.* 2013;8:1–14.
57. Calfa G, Hablitz JJ, Pozzo-Miller L. Network hyperexcitability in hippocampal slices from Mecp2 mutant mice revealed by voltage-sensitive dye imaging. *J Neurophysiol.* 2011;105:1768–84.
58. Contractor A, Klyachko VA, Portera-Cailliau C. Altered neuronal and circuit excitability in fragile X syndrome. *Neuron.* 2015;87:699–715.
59. Balakrishnan S, Mironov SL. Rescue of hyperexcitability in hippocampal CA1 neurons from Mecp2 (-/y) mouse through surface potential neutralization. *PLoS ONE.* 2018;13:1–24.
60. Nelson SB, Valakh V. Excitatory/Inhibitory balance and circuit homeostasis in autism spectrum disorders. *Neuron.* 2015;87:684–98.
61. Sidorov MS, Judson MC, Kim H, Rougie M, Ferrer AI, Nikolova VD, et al. Enhanced operant extinction and prefrontal excitability in a mouse model of Angelman syndrome. *J Neurosci.* 2018;38:2671–82.

62. Wallace ML, Burette AC, Weinberg RJ, Philpot BD. Maternal loss of *Ube3a* produces an excitatory/inhibitory imbalance through neuron type-specific synaptic defects. *Neuron*. 2012;74:793–800.
63. Chen S, Benninger F, Yaari Y. Role of small conductance Ca^{2+} -Activated K^{+} channels in controlling CA1 pyramidal cell excitability. *J Neurosci*. 2014;34:8219–30.
64. Tamir I, Daninos M, Yaari Y. Plasticity of intrinsic firing response gain in principal hippocampal neurons following pilocarpine-induced status epilepticus. *Neuroscience*. 2017;357:325–37.
65. Kuba H, Yamada R, Ishiguro G, Adachi R. Redistribution of $\text{Kv}1$ and $\text{Kv}7$ enhances neuronal excitability during structural axon initial segment plasticity. *Nat Commun*. 2015;6:1–12.
66. Gullledge AT, Bravo JJ. Neuron morphology influences axon initial segment plasticity. *ENeuro*. 2016;3:255–65.
67. Madison DV, Nicoll RA. Control of the repetitive discharge of rat CA1 pyramidal neurones in vitro. *J Physiol*. 1984;354:319–31.
68. Ha GE, Cheong E. Spike frequency adaptation in neurons of the central nervous system. *Exp Neurobiol*. 2017;26:179–85.
69. Tiwari MN, Mohan S, Biala Y, Yaari Y. Differential contributions of Ca^{2+} -activated K^{+} channels and $\text{Na}^{+}/\text{K}^{+}$ -ATPases to the generation of the slow after-hyperpolarization in CA1 pyramidal cells. *Hippocampus*. 2018;28:338–57.
70. Storm JF. After-hyperpolarization of medium duration. *J Physiol*. 1989;409:171–90.
71. Gu N, Vervaeke K, Hu H, Storm JF. $\text{Kv}7/\text{KCNQ/M}$ and HCN/h , but not $\text{KCa}2/\text{SK}$ channels, contribute to the somatic medium after-hyperpolarization and excitability control in CA1 hippocampal pyramidal cells. *J Physiol*. 2005;566:689–715.
72. Castro M-J, Nunes B, De Vries B, Lemos C, Vanmolkot K, Van Den Heuvel J, et al. Two novel functional mutations in the $\text{Na}^{+}/\text{K}^{+}$ -ATPase α 2-subunit *ATP1A2* gene in patients with familial hemiplegic migraine and associated neurological phenotypes. *Clin Genet*. 2007;73:37–43.
73. Al-Mosalem OA, El-Ansary A, Attas O, Al-Ayadhi L. Metabolic biomarkers related to energy metabolism in Saudi autistic children. *Clin Biochem*. 2009;42:949–57.
74. Corti C, Xuereb JH, Crepaldi L, Corsi M, Michielin F, Ferraguti F. Altered levels of glutamatergic receptors and $\text{Na}^{+}/\text{K}^{+}$ ATPase- α 1 in the prefrontal cortex of subjects with schizophrenia. *Schizophr Res*. 2011;128:7–14.